THE JOURNAL OF
PHYSICAL CHEMISTRY C
Article
pubs.acs.org/JPCC

Exploring Rolled-up Au−Ag Bimetallic Microtubes for Surface-Enhanced Raman Scattering Sensor

Yin Yin,[†] Teng Qiu,*[,†] Libo Ma,[‡] Xianzhong Lang,[†] Yan Zhang,[†] Gaoshan Huang,[§] Yongfeng Mei,*[,§] and Oliver G. Schmidt[‡]

[†]Department of Physics, Southeast University, Nanjing 211189, P.R. China
[‡]Institute for Integrative Nanosciences, IFW Dresden, D-01069 Dresden, Germany
[§]Department of Materials Science, Fudan University, Shanghai 200433, P.R. China.

Supporting Information

ABSTRACT: A technique to design and fabricate Au−Ag bimetal microtubes for the investigation of curvature-dependent localized surface plasmon modes is demonstrated. Highly surface-enhanced Raman scattering (SERS) is observed that illustrates the distribution of localized surface plasmon modes leading to an enhanced electromagnetic field. A finite-difference time-domain method is also employed to simulate the electromagnetic field properties on the metal surface. The enhanced SERS performance of such noble bimetal microtubes could spur further interest in the integration of highly sensitive biosensors for rapid, nondestructive, and quantitative bioanalysis, particularly in microfluidics.

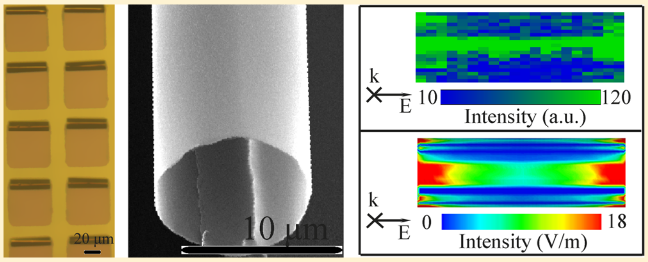

INTRODUCTION

To date, tremendous efforts have been devoted to designing, fabricating, and optimizing functional and versatile nanostructures with desirable sizes, morphologies, and geometrical structures. Strain engineering has gained considerable attention because it offers a methodology to arrange and manipulate nanomembranes into various three-dimensional micro-/nano-architectures ranging from wires[1] and tubes[2,3] to rings[4−6] and wrinkles.[7,8] More recently, self-organized rolled-up tubes on the micro- and nanometer scales based on strain engineering have been developed by releasing strained solid layers from their substrate.[2] Using this method, the nanostructures can be located where they are needed with good control of morphology and structure. In particular, novel functional nanoreactors,[9] injection needles,[10] and nanopipelines[11,12] have been engineered utilizing such rolled-up micro-/nanotubes, allowing for substantial advancements in electronics,[13] magnetics,[14] fluidics,[15,16] photonics,[17,18] and other relevant research fields.[19]

On the other hand, curvature-dependent localized surface plasmon (LSP) modes of noble-metal nanospheroids,[20] nanoshells,[21] and nanorods[22,23] have gained much attention in recent years. Through control of the curvature of nanostructures as a morphologic factor, the distribution of electron density can be tuned, leading to a change in the surface plasmon resonance. In this work, we design and fabricate a curved structure based on Au−Ag bimetal microtubes by employing roll-up nanotechnology. Surface-enhanced Raman scattering (SERS) is observed, which indicates that LSP modes are excited, leading to a largely enhanced local electromagnetic (EM) field when the curved metal surface is irradiated with a laser beam. A finite-difference time-domain (FDTD) method is employed to illustrate the excitation of LSP modes by calculating the EM-field properties on the metal surface. Theoretical simulations also reveal that the tube structures have better performance in the excitation of LSP modes than flat thin nanomembranes and that the LSP modes are also tunable by changing the curvature of the bimetallic microtubes.

Unlike the typical method of generating hot spots in the gap between two closely spaced nanostructures, which results in an enhancement of the local electric field, the microtubes present hot spots located inside their walls that do not originate from any mutual EM interaction. In these functional bimetallic microtubes, the gold layer plays an important role because of its remarkable chemical stability, capability for molecular adhesion, and outstanding biocompatibility. Because gold nanostructures exhibit only a moderate enhancement for SERS detection, we have added a thin silver layer as a good candidate for high surface plasmon resonance excitation efficiency, leading to considerable SERS enhancement. Thus, the Au−Ag bimetal microtubes could bring forward new perspectives toward integration of highly sensitive biosensors for rapid, nondestructive, and quantitative bioanalysis, particularly in microfluidics.

Received: September 6, 2012
Revised: November 9, 2012
Published: November 9, 2012

dx.doi.org/10.1021/jp308854t | *J. Phys. Chem. C* 2012, 116, 25504−25508

EXPERIMENTAL SECTION

Fabrication of Au–Ag Bimetal Microtubes. Au–Ag bimetal microtubes were fabricated by roll-up nanotechnology on a photoresist.[24] The process was initiated by spin-coating a photoresist layer (ARP-3510 positive resist) with a thickness of ∼2 μm onto a Si substrate. Standard photolithography was employed to pattern the photoresist layers into well-defined squares (50 × 50 μm^2) (Figure 1a). Subsequently, thin gold and silver layers were deposited by electron beam evaporation with a tilt angle of 61° (Figure 1b). By employing such a tilted deposition technique, a predefined rolling direction of the nanomembrane was introduced, because a shadow was created at one side of the photoresist edge that provides a well-defined starting line for the formation of rolled-up tubes. Ultimately, the photoresist layer was selectively removed by acetone. Simultaneously, intrinsic stress gradients across the metallic bilayer acted as a driving force to precisely release Au–Ag nanomembranes into rolled-up tubes (Figure 1c). Au–Ag bimetal microtubes were successfully fabricated with controlled film thickness down to <8 nm. We found that, with a thickness of 5 nm for each the silver and gold films, the microtubes were easily rolled up to form well-defined microtube arrays, as shown in Figure 2a.

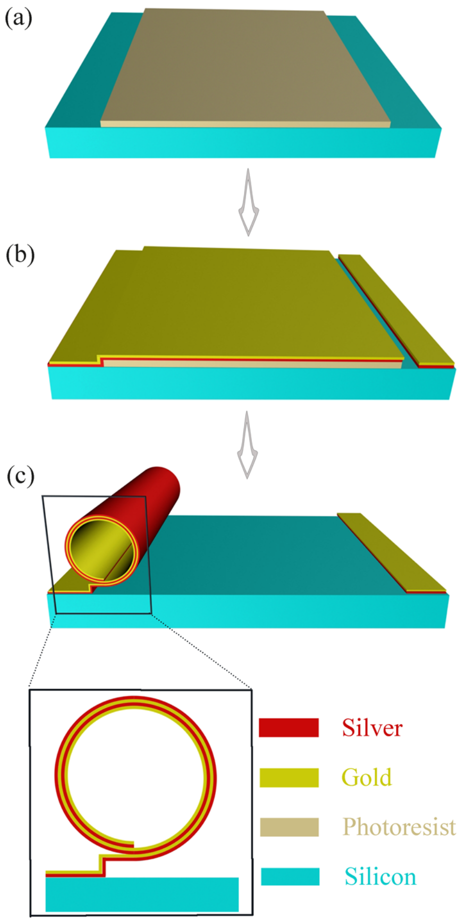

Figure 1. Schematic of the fabrication process of bimetal microtubes. (a) Square photoresist layer on Si substrate. (b) Gold and silver deposited on the photoresist layer by electron beam evaporation with a tilt angle of 61°. (c) Selective removal of the photoresist layer with acetone and rolling up of the the Au–Ag nanomembrane.

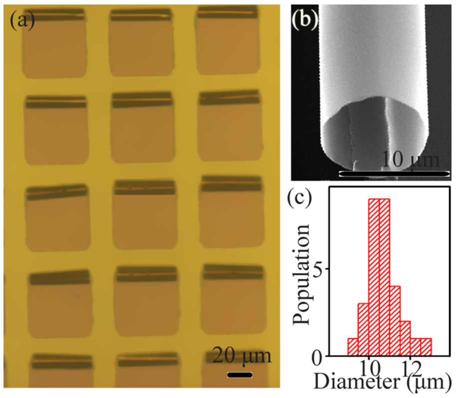

Figure 2. (a) Optical microscopy image of a microtube array patterned into well-aligned squares with the same rolling direction. The layer thicknesses are set to 5 nm for each Ag and Au. (b) SEM image of a typical single microtube with a diameter of ∼10 μm. (c) Statistics of the diameters of bimetal microtubes.

Instrumentation and Data Acquisition. Scanning electron microscopy (SEM, JEOL JSM-6335F) was used to investigate the nanostructures. Raman measurements were performed with a Jobin Yvon LabRAM HR800 micro-Raman spectrometer using a 514-nm laser line at room temperature. An area ∼1 μm in diameter was probed with a 100× objective lens (nominal aperture of 0.45), and the incident power at the sample was 0.04 mW. The signal collection time was 50 s. To evaluate the substrate Raman-enhancing capability, an aqueous solution of rhodamine 6G (R6G) was prepared and dispensed on the samples to facilitate molecular absorption. It should be noted that the acquisition time and laser power were the same for all Raman spectra.

Commercial FDTD software (OptiFDTD 10.0) was used to calculate the EM-field properties of nanostructures. The Drude model was employed to describe the properties of silver and gold. The parameters of the bimetal microtubes in the simulation were set to the parameters in our experiments. The height of the calculation area was set to 30 μm, and the light source was set at the top of the calculation area, 10 μm from the top surface of the microtube. A linear incident wave was used, and the electric field strength of the incident wave was set to 1 V/m. The wavelength of the incident wave was set to 514 nm. Perfectly matched layer boundary conditions were applied to simulate the absorbing boundary.

RESULTS AND DISCUSSION

A typical optical microscopy image of microtube arrays patterned into well-aligned squares with the same rolling direction is shown in Figure 2a. The ability to align tubes in a highly ordered manner demonstrates that variously shaped tube patterns can be readily constructed by controlling the geometries and positions of the photoresist layers by standard photolithography processes.[25] Moreover, employing polymer as the photoresist layer allows for simple removal of the underlying sacrificial layer without dissolution of the nanomembrane material itself during the underetching process. A tunable bimetal film thickness can be achieved by varying the deposition time of electron beam evaporation, and the number of rotations of bimetal microtubes varying with the etching time also provides an advantage in tailoring the structure of the microtube. Figure 2b shows an SEM image of a typical single microtube. We carried out a statistical analysis of the microtubes and found that the diameters of microtubes are mainly located at around ~10 μm (Figure 2c). This indicates that good reproducibility can be achieved in our experiments when the experimental fabrication parameters are sufficiently well controlled. Moreover, strong built-in strain gradients inside the thin bimetal membrane primarily drive the roll-up of the layers. The driving force for tube formation can be controlled by changing the deposition parameters, such as growth rate and substrate temperature.[24]

To evaluate the substrate Raman-enhanced signal, a measurement of the SERS capability of the bimetal microtube was carried out, and the excitation efficiency of LSP modes on the curved metal surface was evaluated. We prepared a 1×10^{-4} M aqueous solution of R6G and put droplets on the tubes to facilitate molecular absorption. Figure 3a shows typical Raman spectra of R6G molecules absorbed on the bimetal microtube at position A (see inset) and on a flat bimetal reference nanomembrane. Many salient peaks were clearly observed when the R6G molecules were absorbed on the bimetal microtube, and the pronounced peaks at 1507, 1574, and 1650 cm^{-1} can be assigned to the totally symmetric modes of in-plane C−C stretching vibrations.[26] Obviously, a comparison between the intensity of the Raman peaks of R6G on the microtube and on the flat nanomembrane suggests that the curved surface provides Raman enhancement, which, in turn, indicates that more LSP modes were excited on the metal surface of the microtube than on the flat nanomembrane. For another cross-check, we carried out identical measurements on a SiO$_x$-based tube (without any silver) and did not observe any enhanced Raman signal. Different positions on the microtube surface were found to cause different degrees of Raman enhancement. We chose three different positions (see inset) for Raman measurements: position A (near the end of the microtube), position B (top area), and position C (side face). Figure 3b shows the Raman intensities of the band at 1650 cm^{-1} for positions A, B, and C. The enhancement near the end of the microtube is larger than that at the side face and top area, which suggests that different distributions of LSP modes are found on the curved metal surface. Moreover, a rough estimation yields a surface enhancement factor (EF) of 10^4 based on the quantitative intensity of the Raman signal of the selected band at 1650 cm^{-1} in spectrum A. However, as reported earlier, R6G absorbed on a flat silver layer deposited on a Si substrate exhibited no recognizable Raman signatures.[27]

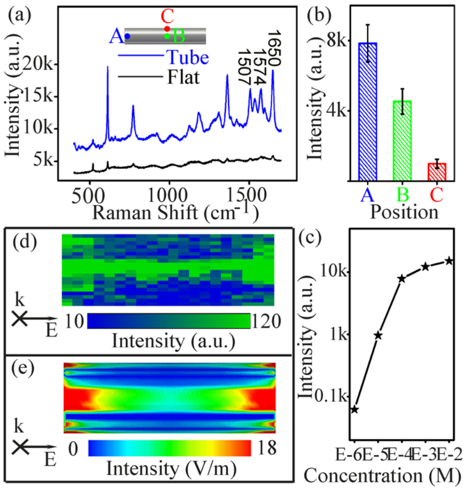

Figure 3. (a) Raman spectra of R6G molecules absorbed on the end of a bimetal microtube (position A) and a flat bimetal nanomembrane. (b) Raman intensities of R6G molecules absorbed on different positions of the microtube surface. The inset in panel a shows the different positions of the Raman measurements, namely, at the open tube end (position A), top area (position B), and side face (position C) of the microtube. (c) Average SERS signal at 1650 cm^{-1} at the end of a microtube as a function of R6G solution concentrations. (d) Raman intensity mapping (10×50 μm^2) obtained from the integrated intensity of the 1650 ± 10 cm^{-1} band of 10^{-4} M R6G adsorbed on the surface of the microtube. (e) Simulated EM-field distribution map of the bimetal microtube surface.

Solutions of R6G with different concentrations were also used to study the SERS dynamic range of the bimetal microtube. Figure 3c shows the recorded Raman intensity at 1650 cm^{-1} at the open end of the microtube (position A) as a function of solution concentration varied from 1×10^{-6} to 1×10^{-2} M. Linear behavior is observed from 1×10^{-6} to 1×10^{-4} M with a proportionality constant of unity, which suggests that the number of adsorption sites with high Raman enhancement is large enough to accommodate a considerable range of sample concentrations. When the concentration was increased to more than 1×10^{-4} M, nonlinear saturation emerged. This indicates that the adsorption sites for R6G moelcules with high enhancement became less available and stacks of R6G molecules were more likely. As a result, the high EF of the Raman features generated by the rolled-up microtubes with an outermost silver layer surface and the broad dynamic range for investigating different concentrations of solutions make such tube structures potentially useful for the sensing and analysis of chemical and biological molecules by SERS.

To obtain more details, two-dimensional point-by-point SERS mapping was performed to evaluate the distribution of enhanced intensity across the rolled-up bimetal microtube, which is shown in Figure 3d. The map was obtained from the integrated intensity of the 1650 ± 10 cm^{-1} band of a 1×10^{-4} M R6G aqueous solution on the surface of the microtube. A mapping area of 10×50 μm^2 was acquired by measuring 20×20 points with a regular longitudinal scanning step of 0.5 μm and a transverse scanning step of 2.5 μm. The top area of the microtube surface acquired stronger Raman intensity than the two side faces. The enhanced intensity was almost the same along the axis of the tube except for the two ends, where the Raman signal was much stronger. Different distributions of intensity in the Raman mapping can be attributed to different distributions of the EM field near the tube surface where LSP modes have been excited by the interaction between the incident light and the free electrons on the metal surface.

To assess the validity of our measurements, an FDTD method was employed to calculate the local EM field, as shown in Figure 3e. The intensity distribution from the simulation is fairly consistent with the results of experimental Raman mapping. When irradiated by a laser beam, the LSP modes on the metal surface lead to a larger EM field, in turn causing a significant Raman enhancement. The enhanced EM field near the top area was apparently larger under the laser beam vertically irradiating the top surface, whereas on the side faces, the interaction between incident light and free electrons on the metal surface was not as efficient as that on the top. Along the axis of the tube, the area near the two tubes ends exhibited the maximum intensity of the local EM field E_{loc}; the calculated result of E_{loc} near the tube surface was about 18 V/m, and the electric field intensity of the incident light, E_0, was assumed to be 1 V/m. As a result, the maximum EF could be as high as

$>10^5$ according to the simple equation EF = $(E_{\text{loc}}/E_0)^4$.[28] The difference between the experimental EF (10^4) and the simulated EF (10^5) is mainly attributed to both imperfections of the actual experimental tube shape and structure and a decay of the R6G molecule emission efficiency during the measurements. Importantly, unlike the usual method of generating hot spots in the gap between two closely spaced nanostructures, which results in an enhancement of the local electric field, the microtubes present hot spots within their curved walls that are not caused by any mutual EM interaction. As a result, with the high EF of the EM field on their surface, the rolled-up bimetal microtubes offer new possibilities toward sensing by SERS in chemical analysis and cell biology.

The influence on the local EM field introduced by different curvatures based on Au−Ag microtubes was also studied by simulations. Figure 4 shows the EM-field distribution on bimetal microtubes with different curvatures of (a) 0.100, (b) 0.033, (c) 0.020, (d) 0.010, and (e) 0 μm^{-1}. The considered curvature in Figure 4a corresponds to that of the microtubes in our experiments. It should be noted that the scale bars of the simulated EM fields are different in each of the five panels. By comparison, we can conclude that, with decreasing curvature, the intensity of the excited EM field near the surface reduces, which means that the excitation efficiency of the LSP modes is lower. The minimum local EM field occurs for the flat metal surface (with a curvature of 0). These results open a practical route toward achieving a tunable surface plasmon resonance by simply changing the curvature of bimetal microtubes.

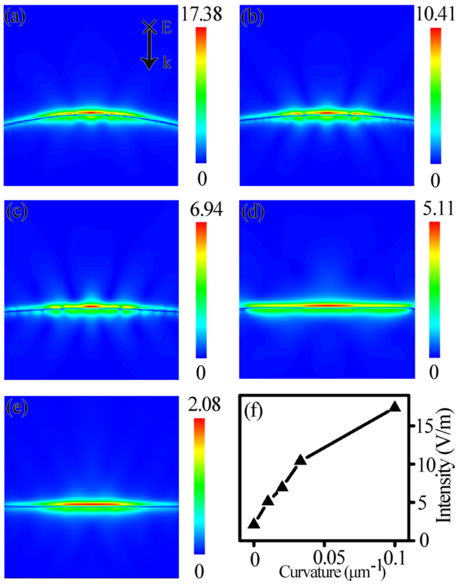

Figure 4. Simulated EM-field distributions on the surfaces of bimetal microtubes with different curvature: (a) 0.100, (b) 0.033, (c) 0.020, (d) 0.010, and (e) 0 μm^{-1}. (f) Simulated maximum EM-field intensity as a function of microtube curvature.

CONCLUSIONS

In summary, we have reported a technique to design and fabricate a curved structure based on Au−Ag bimetal microtubes. Pronounced SERS was observed, indicating that LSP modes can be excited in the tubes that lead to a greatly enhanced local EM field. FDTD simulations illustrate the excitation of LSP modes by calculating the EM-field properties on the metal surface. The theoretical simulations also reveal that curved micro-/nanostructures are very efficient in exciting LSP modes and that one can achieve a tunable surface plasmon resonance by changing the curvature of bimetal microtubes. The high Raman enhancement effect suggests that these bimetal microtubes represent excellent candidates for the integration of highly sensitive biosensors for rapid, nondestructive, and quantitative bioanalysis, particularly in microfluidics.

ASSOCIATED CONTENT

Supporting Information

SEM images of bimetal microtubes, UV−vis spectra of a bimetal microtube array and a flat bimetal nanomembrane, and simulation results of the absorption spectrum of a rolled-up Ag−Au mutilayer. This material is available free of charge via the Internet at http://pubs.acs.org.

AUTHOR INFORMATION

Corresponding Author

*E-mail: tqiu@seu.edu.cn (T.Q.) and yfm@fudan.edu.cn (Y.M.).

Notes

Notes. The authors declare no competing financial interest.

ACKNOWLEDGMENTS

T.Q. acknowledges support from the National Natural Science Foundation of China under Grants 51271057 and 51071045; the Program for New Century Excellent Talents in University of Ministry of Eduction of China under Grant NCET-11-0096; the Natural Science Foundation of Jiangsu Province, China, under Grant BK2012757; and the open research fund of Key Laboratory of MEMS of Ministry of Education, Southeast University. Y.F.M. and G.S.H. thank the Natural Science Foundation of China (Nos. 61008029, 51102049), the Program for New Century Excellent Talents in University (No. NCET-10-0345), and the Shanghai Pujiang Program (No.11PJ1400900).

REFERENCES

(1) Kumar, A.; Fähler, S.; Schlörb, H.; Leistner, K.; Schultz, L. *Phys. Rev. B* **2006**, *73*, 064421.

(2) Schmidt, O. G.; Eberl, K. *Nature* **2001**, *410*, 168.

(3) Schmidt, O. G.; Schmarje, N.; Deneke, C.; Müller, C.; Jin-Phillipp, N. Y. *Adv. Mater.* **2001**, *13*, 756−759.

(4) Schmidt, O. G.; Deneke, C.; Schmarje, N.; Müller, C.; Jin-Phillipp, N. Y. *Mater. Sci. Eng, C* **2002**, *19*, 393−396.

(5) Zhang, L.; Dong, L. X.; Nelson, B. L. *Appl. Phys. Lett.* **2008**, *92*, 143110.

(6) Urena, E. B.; Mei, Y. F.; Coric, E.; Makarov, D.; Albrecht, M.; Schmidt, O. G. *J. Phys. D: Appl. Phys.* **2009**, *42*, 055001.

(7) Mei, Y. F.; Thurmer, D. J.; Cavallo, F.; Kiravittaya, S.; Schmidt, O. G. *Adv. Mater.* **2007**, *19*, 2124−2128.

(8) Mei, Y. F.; Kiravittaya, S.; Benyoucef, M.; Thurmer, D. J.; Zander, T.; Deneke, C.; Cavallo, F.; Rastelli, A.; Schmidt, O. G. *Nano Lett.* **2007**, *7*, 1676−1679.

(9) Deneke, C.; Jin-Phillipp, N. Y.; Loa, I.; Schmidt, O. G. *Appl. Phys. Lett.* **2004**, *84*, 4475−4477.

(10) Prinz, V. Y. *Microelectron. Eng.* **2003**, *69*, 466−475.

(11) Schmidt, O. G.; Jin-Phillipp, N. Y. *Appl. Phys. Lett.* **2001**, *78*, 3310−3312.

(12) Deneke, C.; Schmidt, O. G. *Physica E* **2004**, *23*, 269−273.

(13) Cavallo, F.; Songmuang, R.; Schmidt, O. G. *Appl. Phys. Lett.* **2008**, *93*, 143113.

(14) Müller, C.; Khatri, M. S.; Deneke, C.; Fähler, S.; Mei, Y. F.; Urena, E. B.; Schmidt, O. G. *Appl. Phys. Lett.* **2009**, *94*, 102510.
(15) Deneke, C.; Schmidt, O. G. *Appl. Phys. Lett.* **2004**, *85*, 2914−2916.
(16) Thurmer, D. J.; Deneke, C.; Mei, Y. F.; Schmidt, O. G. *Appl. Phys. Lett.* **2006**, *89*, 223507.
(17) Deneke, C.; Schmidt, O. G. *Appl. Phys. Lett.* **2006**, *89*, 123121.
(18) Schwaiger, S.; Broll, M.; Krohn, A.; Stemmann, A.; Heyn, C.; Stark, Y.; Stickler, D.; Heitmann, D.; Mendach, S. *Phys. Rev. Lett.* **2009**, *102*, 163903.
(19) Songmuang, R.; Deneke, C.; Schmidt, O. G. *Appl. Phys. Lett.* **2006**, *89*, 223109.
(20) Kooij, E. S.; Ahmed, W.; Zandvliet, H. J. W.; Poelsema, B. *J. Phys. Chem. C* **2011**, *115*, 10321−10332.
(21) Krohne., N. P.; Novikov, S. M.; Beermann, J.; Morgen, P.; Bozhevolnyi, S. I.; Albrektsen, O. *Opt. Express* **2011**, *20*, 534−546.
(22) Grzelczak, M.; Sanchez, I. A.; Rodriguez, G. B.; Alvarez, P. R.; Perez, J. J.; Liz, M. L. M. *Adv. Funct. Mater.* **2008**, *18*, 3780−3786.
(23) Jiao, Z.; Xia, H.; Tao, X. *J. Phys. Chem. C* **2011**, *115*, 7887−7895.
(24) Mei, Y. F.; Huang, G. S.; Solovev, A. S.; Ureña, E. B.; Mönch, I.; Ding, F; Reindl, T.; Fu, R. K. Y.; Chu, P. K.; Schmidt, O. G. *Adv. Mater.* **2008**, *20*, 4085−4090.
(25) Huang, G. S.; Kiravittaya, S.; Bolanos Quinones, V. A.; Ding, F.; Benyoucef, M.; Rastelli, A.; Mei, Y. F.; Schmidt, O. G. *Appl. Phys. Lett.* **2009**, *94*, 141901.
(26) Hildebrandt, P.; Stockburger, M. *J. Phys. Chem.* **1984**, *88*, 5935−5944.
(27) Gunnarsson, L.; Bjerneld, E. J.; Xu, H.; Petronis, S.; Kasemo, B.; Käll, M. *Appl. Phys. Lett.* **2001**, *78*, 802−804.
(28) Qiu, T.; Zhang, W.; Lang, X.; Zhou, Y.; Cui, T.; Chu, P. K. *Small* **2009**, *5*, 2333−2337.